SUPPORTING INFORMATION

Resolving the adsorption of molecular O_2 on the rutile $TiO_2(110)$ surface by non-contact atomic force microscopy

Igor Sokolović,[1] Michele Reticcioli,[1,2] Martin Čalkovský,[1,3] Margareta Wagner,[1,4]
Michael Schmid,[1] Cesare Franchini,[2,5,*] Ulrike Diebold,[1] and Martin Setvín[1,6,†]

[1]*Institute of Applied Physics, TU Wien, Wiedner Hauptstraße 8-10/134, 1040 Vienna, Austria*
[2]*University of Vienna, Faculty of Physics and Center for Computational Materials Science, Vienna, Austria*
[3]*Institute of Physical Engineering, Brno University of Technology, Technická 2896/2, 616 69 Brno, Czech Republic*
[4]*CEITEC – Central European Institute of Technology, Brno University of Technology, Purkyňova 123, 612 00 Brno, Czech Republic*
[5]*Dipartimento di Fisica e Astronomia, Università di Bologna, 40127 Bologna, Italy*
[6]*Department of Surface and Plasma Science, Faculty of Mathematics and Physics, Charles University, V Holešovičkách 2, 180 00 Prague 8, Czech Republic*

CONTENTS

S 1. Adsorption energy dependence on the distance from the V_O 1

S 2. Calculated O_2 adsorption with excess electrons 2

S 3. Comparing calculated superoxo and peroxo species with experiments 3

S 4. Constant-current STM 4

S 5. Tip-induced rotation of a $\boldsymbol{\tau}$ molecule 5

S 6. Simulation of the force-distance $\boldsymbol{F(z)}$ curves 6

S 7. Simulated $\boldsymbol{F(z)}$ curves without van der Waals corrections 7

S 8. Simulated $\boldsymbol{F(z)}$ curves with an inclined tip 8

S 9. Diffusion under UV irradiation 9

S 10. $In_2O_3(111)$ surface imaged with the functionalized AFM tip 10

S 11. SI videos 11

References 11

---

* cesare.franchini@univie.ac.at
† setvin@iap.tuwien.ac.at

www.pnas.org/cgi/doi/10.1073/pnas.1922452117

S 1. ADSORPTION ENERGY DEPENDENCE ON THE DISTANCE FROM THE V_O

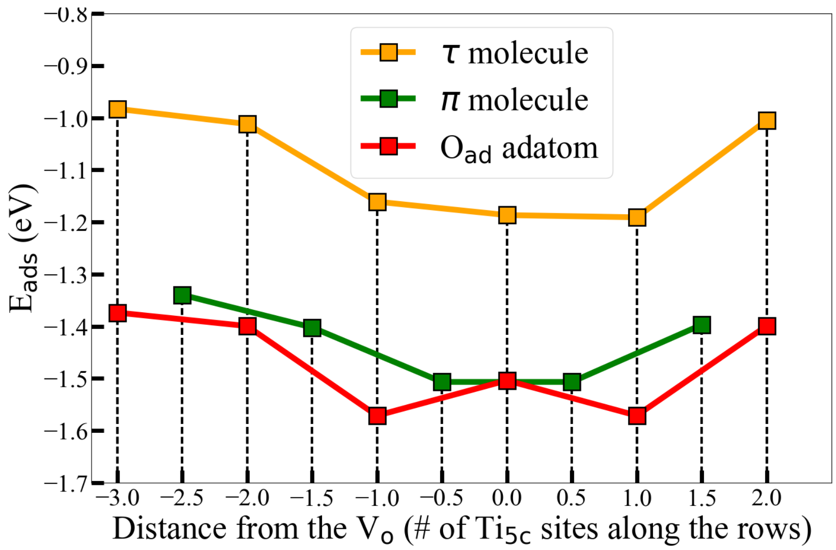

FIG. S 1: **Adsorption energy dependence of different oxygen species with respect to the distance from the V_O.** The plot shows the adsorption energies of π, τ and O_{ad} species adsorbed at different locations from the position of an V_O in a periodic (6×2) slab.

Figure S1 shows the dependence of the adsorption energy E_{ads} of adsorbed oxygen in different configurations as a function of the distance along [001] from the empty oxygen vacancy in the surface slab. The calculations were performed on a slab with one empty oxygen vacancy, *i.e.* the slab used for the calculations in Figures 1c–1g of the main text.

The distance-dependence of the adsorbed species shows an attractive interaction between the adsorbate and the V_O (as expected for species with opposite charge), with a saturating trend further away from the V_O. The variation is less than 10% of the highest adsorption energy (the lowest value of E_{ads}) for each species. This distance dependence is not too pronounced, as confirmed experimentally in the AFM images in the main text: The adsorbed molecules show no obvious correlation with the position of oxygen vacancies. The existence of isolated O_{ad} is solely due to the vacancy-mediated dissociation channel, which leaves an O_{ad} on Ti_{5c} and one O_{br} to heal the vacancy. Thus, for oxygen adatoms created by dissociation of the ω molecule in oxygen vacancies, the position is necessarily related to the position of the V_O where it originates from. Dissociation puts these O_{ad} directly adjacent to the V_O [1]; diffusion to the energetically more favorable nearest-neighbor position with regard to the oxygen vacancy is hindered at low temperatures.

The π molecule shows a symmetric energy-distance curve in Fig. S1 with the degenerate position of the minimum, since this molecule is bound to two underlying lattice Ti_{5c} atoms. The adsorption energy vs. position of the τ molecule is not symmetric due to the directional character of this molecule: the molecule prefers to orient one of its constituent O atoms towards the empty V_O due to electrostatic attraction of the negative O atom and the positive V_O. Therefore, it prefers adsorption on one Ti_{5c} away from the vacancy to being adsorbed directly next to a vacancy.

S 2. CALCULATED O_2 ADSORPTION WITH EXCESS ELECTRONS

E_{ads}	no added e^-	1 added e^-	2 added e^-
τ	+3.36	+0.98	-1.01
π	+3.17	-0.75	-1.49
O_{ad}	+1.72	+0.07	-1.58

FIG. S 2: **Adsorption energies (in eV) of O_2 and O_{ad} as a function of electron doping**. The table shows adsorption energies of different molecular and atomic oxygen species when they are adsorbed to a slab with the oxygen vacancy occupied by an ω molecule.

Fig. S2 is a table showing the stability of adsorbates as a function of electron doping. In the non-reduced surface slab (no excess electrons) the V_O is populated with an ω molecule. These calculations are simulating the observed adsorption after O_2 exposure to a surface at 80 K, where all the oxygen vacancies are populated by the energetically most favorable ω molecules. Then, all the polaronic electrons are transfered to the ω^{2-} molecules and the surface has no further electrons to donate to additional O_2 molecules. Therefore, no chemisorption occurs without addition of excess electrons (first column).

For further chemisorption to occur, additional electron doping is required. The excess electrons introduced to the slab (with a uniform positive background to keep overall charge neutrality) tend to localize on the additional O_2 molecule on the Ti_{5c} row. The resulting, stable solutions are non-metallic.

Addition of only one electron to a non-reduced slab will stabilize only the π molecules in the superoxo charge state, while the other species do not adsorb (second column).

When two electrons are added to a slab with the oxygen vacancy, still populated by an ω^{2-} molecule, an additional molecule can be adsorbed to the surface (third column). The additional, chemisorbed molecule or adatom has roughly the same adsorption energy as a single peroxo molecule adsorbed to a reduced slab. Also the other properties of the molecules adsorbed this way are the same as shown in Fig. 1 of the main text.

S 3. COMPARING CALCULATED SUPEROXO AND PEROXO SPECIES WITH EXPERIMENTS

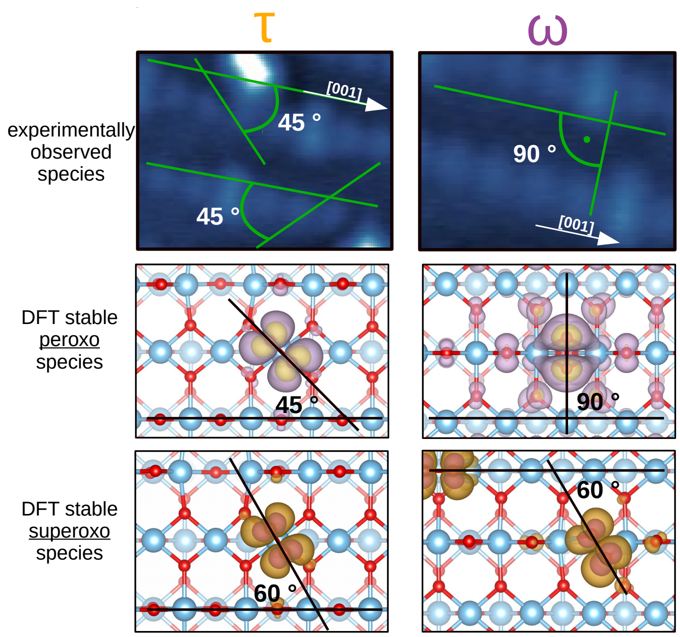

FIG. S 3: **Comparison of calculated superoxo and peroxo ω and τ species geometries with experimentally observed geometries.** Geometry of the molecular τ (left column) and ω (right colum) species in experiment (top row), calculated peroxo state (middle row), and calculated superoxo state (bottom row).

The chemically inert oxygen-terminated tip does not provide direct information on the charge state of the adsorbed molecules; we do not see significant differences in the frequency shift above different molecules adsorbed at equivalent sites. Therefore, we compare the geometry of calculated species with the geometry of experimentally observed species to identify whether the adsorbed molecules are superoxo or peroxo species.

Fig. S3 shows the experimental and calculated geometries of τ and ω molecules. In experiments, the τ molecules are always rotated by 45° towards the O_{br} rows, while ω molecules are always perpendicular to the O_{br} rows (top row of Fig. S3). Calculated superoxo τ and ω species show a rotation by 60° with respect to the [001] axis. On the other hand, calculated peroxo τ molecules are rotated by 45° and the ω molecules are perpendicular to the O_{br} rows. The angles of the calculated peroxo τ and superoxo τ are not dependent on the distance from the V_O in calculations, and consistently relax to 45° and 60° with respect to the [001] axis, respectively. Therefore, we assign the experimentally observed τ and ω species to the peroxo charge state.

The geometry of the π molecule does not allow for similar, direct comparisons of experiment and theory. We can only state that we have not observed any preference for the appearance of π and τ molecules on the surface, making them equivalent during adsorption and similar in properties. Therefore, we conclude that π molecules are peroxo as well.

S 4. CONSTANT-CURRENT STM

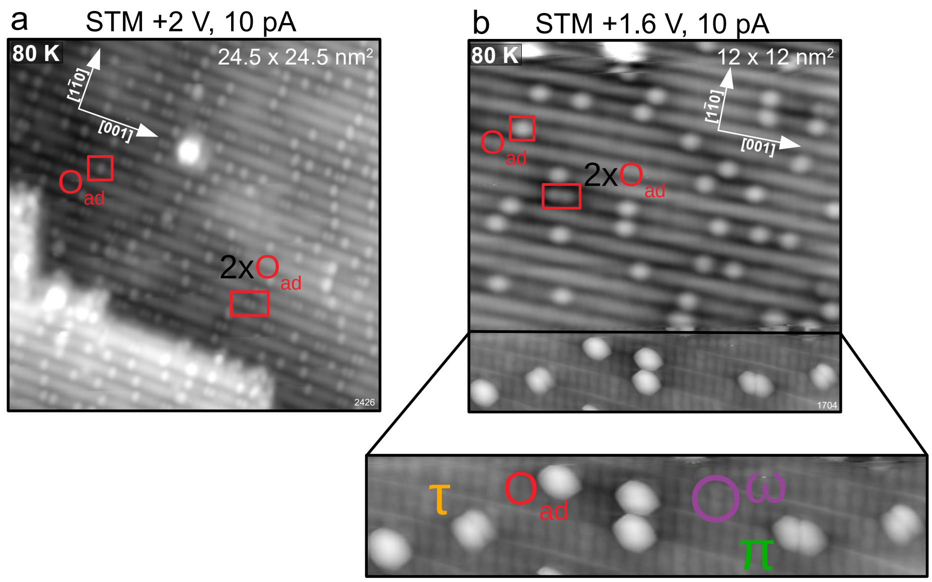

FIG. S 4: **Constant-current STM images of the O_2 covered surface at 78 K.** a) Typical large-area STM image showing products of electron-induced O_2 dissociation. b) Smaller-area STM image showing the typical STM contrast in the top part of the image and a rare contrast at the bottom (enlarged below).

Figures 5 and 6 of the main text show how electron injection or removal affects the adsorbed molecules. Fig. S4 shows constant-current STM images of the positively biased sample (with respect to the grounded tip), *i.e.* empty-states STM images. The electrons are injected into the unoccupied states on the surface and subsequently dissociate all molecular species.

Fig. S4a is a large-area image showing the typical empty-states STM contrast on this surface: Ti_{5c} rows are imaged as protrusions and O_{br} rows as depressions. The dark O_{br} rows are featureless and show no presence of ω molecules or oxygen vacancies. Similarly, the bright Ti_{5c} rows show neither π nor τ molecules. The Ti_{5c} rows are covered with either single O_{ad} originating from the tip-induced dissociation of ω molecules, or paired O_{ad} features originating from the tip-induced dissociation of π or τ molecules.

Fig. S4b shows a smaller-area STM image with two distinct contrasts in the image and one tip-change event. The top of Fig. S4b shows a typical STM contrast with atomic resolution on O_{ad}, same as in Fig. S4a. The bottom of Fig. S4b is enlarged in the inset and shows a rare STM contrast in which the O_{br} rows are atomically resolved and bright, while the Ti_{5c} rows are imaged as thin lines. Additionally, all the adsorbates are visible and recognized with atomic resolution in this STM contrast, marked in the inset of Fig. S4b. This type of contrast is attributed to a barely conducting tip, which had to be approached very close to the surface. At such proximity, the STM imaging contrast is affected by the tip-surface interactions, and the STM images carry similar information as the AFM images. This type of tip decoration is not stable when imaging this surface and the tip-change occurs quickly (Fig. S4b is imaged bottom-up).

Both STM images in Fig. S4 illustrate the advantages of studying the O_2 adsorption using nc-AFM instead.

S 5. TIP-INDUCED ROTATION OF A τ MOLECULE

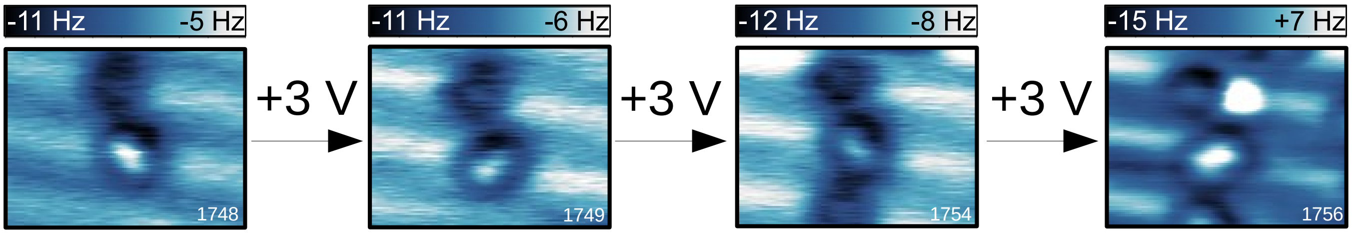

FIG. S 5: **Sequence of images showing tip-induced rotation of a single τ molecule.** A positive-bias ramp from 0 V to +3 V was performed above the molecule between successive frames of the figure.

Dissociation of τ molecules by electron injection appears to be the least probable molecular dissociation channel, see Fig. 5 of the main text. Unlike π and ω molecules, which dissociate at much smaller bias voltages, the τ molecules either dissociate or simply rotate when a bias larger than +3 V is applied above them.

Fig. S5 shows a series of AFM images showing the rotation of a single τ molecule. Between successive images, a positive-bias ramp was performed above the molecules in the same way as in the Fig. 5e of the main text. The process of rotation can be performed until the molecule finally dissociates. This series of experiments confirms the robustness of τ molecules to electron injection, noticeable by comparing Figures 5a and 5b of the main text as well.

S 6. SIMULATION OF THE FORCE-DISTANCE $F(z)$ CURVES

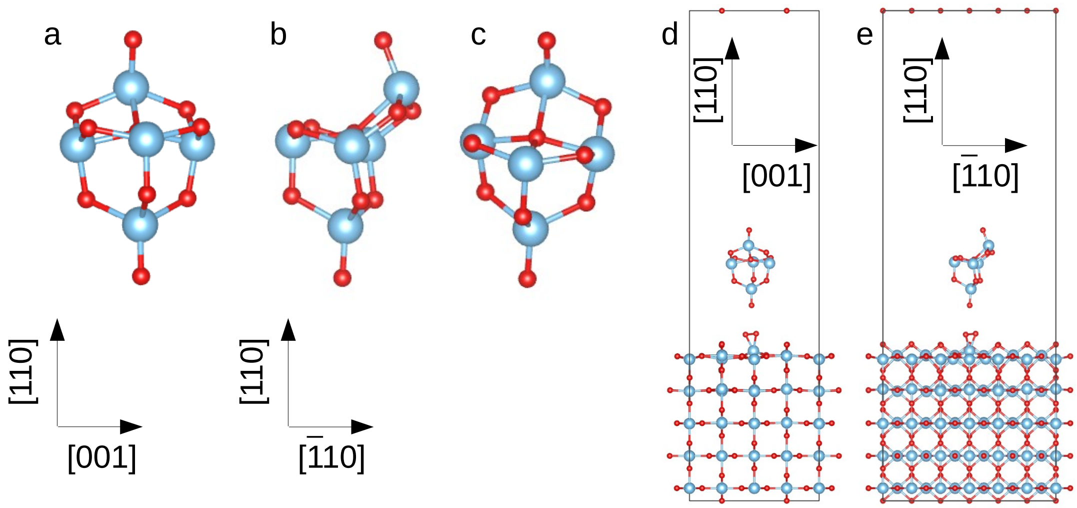

FIG. S 6: **Ball-and-stick model of the simulated AFM tip and the setup for simulated force-distance curves.** The tip model viewed from the a) front, b) side and c) in 3 dimensions. d,e) Setup for simulation of the F(z) curves viewed from the front (d) and the side (e).

The approach of the AFM tip to the adsorbed species is visualized in the simulated $F(z)$ movies that can be downloaded from the online supplement of this paper. At each point of the tip approach, the force is measured as a sum of forces acting on the atoms of the simulated AFM tip.

At low tip-sample distances, both, the tip and the adsorbate start to deform. When the tip is sufficiently close, the chemical attraction between the bottom Ti atom of the tip with the surface O atoms becomes relevant. The simulated force-distance curves in the main text are limited to the range where no strong deformations of either tip or the adsorbates occur. In all cases, the tip was positioned above one of the oxygen atoms within the molecule. Placing the tip in the centre of the molecule resulted in additional tilting or molecule dissociation in some cases.

S 7. SIMULATED $F(z)$ CURVES WITHOUT VAN DER WAALS CORRECTIONS

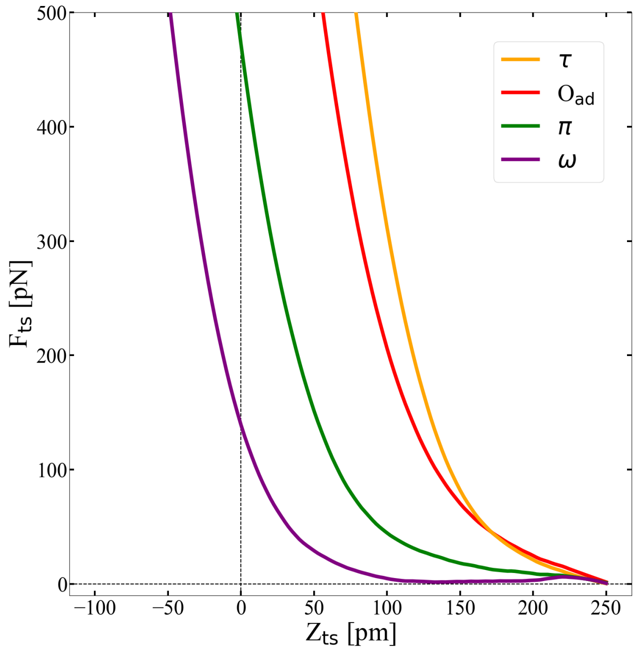

FIG. S 7: **Simulated $F(z)$ curves without van der Waals corrected functionals.** The curves were obtained with an indentical procedure as in Fig. 7c of the main text, except for the exclusion of the van der Waals corrected functionals in each point of the approach.

The simulated $F(z)$ curves without the van der Waals corrections in the DFT calculations show no attractive minima in the tip-adsorbate interaction. The calculations with van der Waals forces (Fig. 7c in the main text) shows clearly defined, although shallow, attraction basins. Therefore, we conclude that the attraction seen in the experimental $F(z)$ stems from the van der Waals forces between the atoms terminating the AFM tip and the adsorbate-covered surface.

S 8. SIMULATED $F(z)$ CURVES WITH AN INCLINED TIP

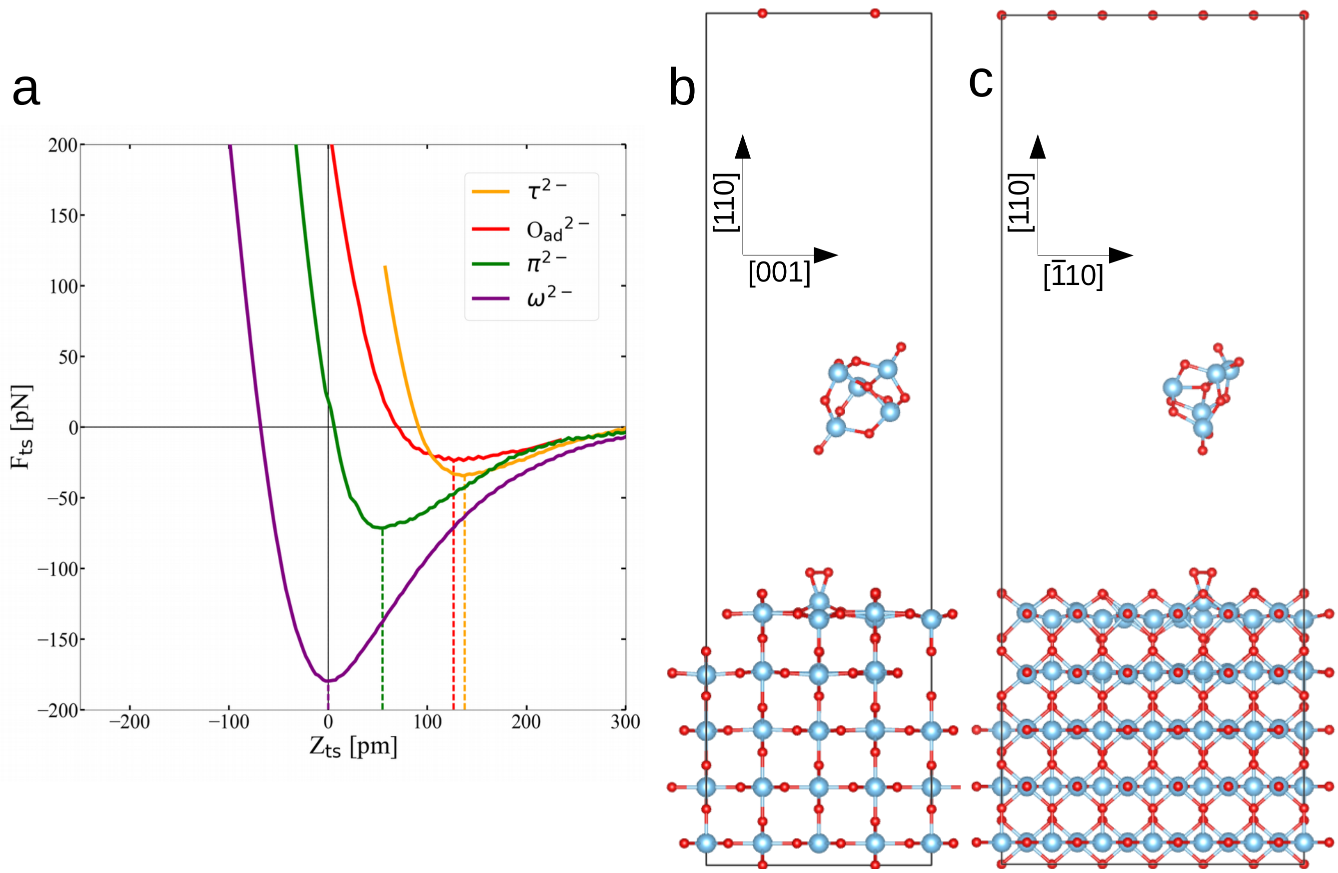

FIG. S 8: **Simulated $F(z)$ curves with a tip inclined towards the surface.** a) Resulting $F(z)$ curves showing deeper attraction basins when compared to Fig. 7c of the main text. b) front view and c) side view of the setup for simulating $F(z)$ curves shown in (a).

When the $F(z)$ curves are simulated with a differently oriented AFM tip, the resulting curves are slightly different than the curves obtained with the same tip in normal orientation towards the surface (Fig. 7c of the main text).

The tip in Fig. S8 is inclined towards the surface, exposing more of its constituent atoms to the surface. The van der Waals force between the tip atoms and the surface is therefore increased, and the $F(z)$ curves have deeper attraction minima, as can be seen in Fig. S8a. The increase in attraction is most noticeable in the $F(z)$ curve above the ω molecule, where the tip is approached closest to the surface before the onset of repulsion.

It was indeed observed experimentally that some tips exhibited such stronger interaction. The rearrangement of the atoms at the tip apex is highly probable in experiments, but the oxygen at the tip apex is nevertheless responsible for the excellent lateral resolution and the absence of chemical interaction with the surface.

S 9. DIFFUSION UNDER UV IRRADIATION

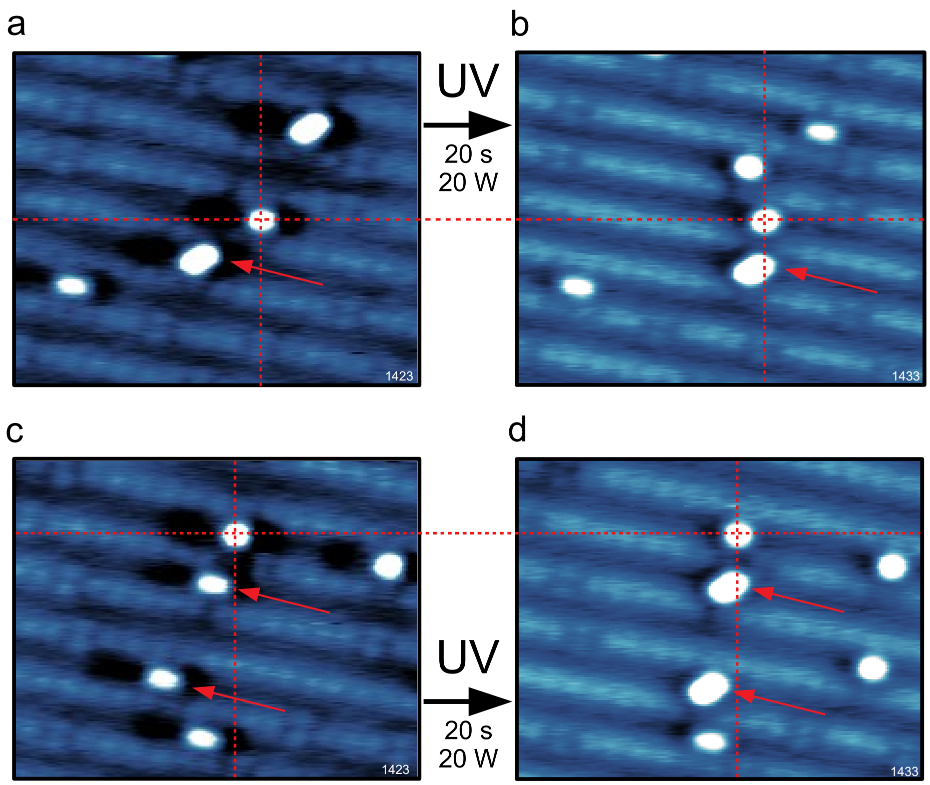

FIG. S 9: **UV-induced diffusion of π and τ molecules.** a,c) Constant-height AFM images of the surface prior to UV irradiation. b,c) Constant height AFM images of the surface after 20 s of 20 W UV irradiation: Panel a) and c) are (3x) enlarged parts of Fig. 4a of the main text, while panels b) and d) are enlarged parts of Fig. 4b of the main text.

We discuss the possible reactions under UV illumination in the main text. Here, we show a more detailed view on a process not as fundamental as the ones described in the main text: diffusion of the π and τ molecules. Here, as well as in the main text, we use a photo-blind O_{ad} as a reference, marked by the intersection of red, broken lines in Fig. S9.

Figures S9a and S9b focus on the evolution of a τ molecule before and after 20 s of 20 W of UV irradiation. Even though the τ molecule has not been desorbed or transformed to a π molecule, we observe that it has shifted its position two unit cells closer to the reference O_{ad}. We argue that the processes described in the main text, *i.e.*, the single-step or the two-step process, are responsible for this behavior: The τ molecule first accepts a UV-generated hole to become an unstable superoxo O_2^-, and subsequently captures an electron to return to the stable peroxo state. However, during this process, the molecule has strengthened its bonds to lattice Ti_{5c} (s), which do not have to coincide with the original bonds to the substrate. This molecule has effectively moved two unit cells at temperatures of 80 K, by transforming to the unstable superoxo and readsorbing back to the stable peroxo state in a new configuration.

A similar example is seen when comparing Figures S9c and S9d, which focus on two π molecules before and after 20 s of 20 W of UV irradiation. Both π molecules have transformed to a τ molecule. However, one has moved one unit cell further than the other one. The longer translation of one molecule can be either because this molecule had undergone more transformation processes (at least one reaction more), or because the metastable superoxo O_2^- species is mobile on the surface and can diffuse several unit cells.

S 10. IN_2O_3(111) SURFACE IMAGED WITH THE FUNCTIONALIZED AFM TIP

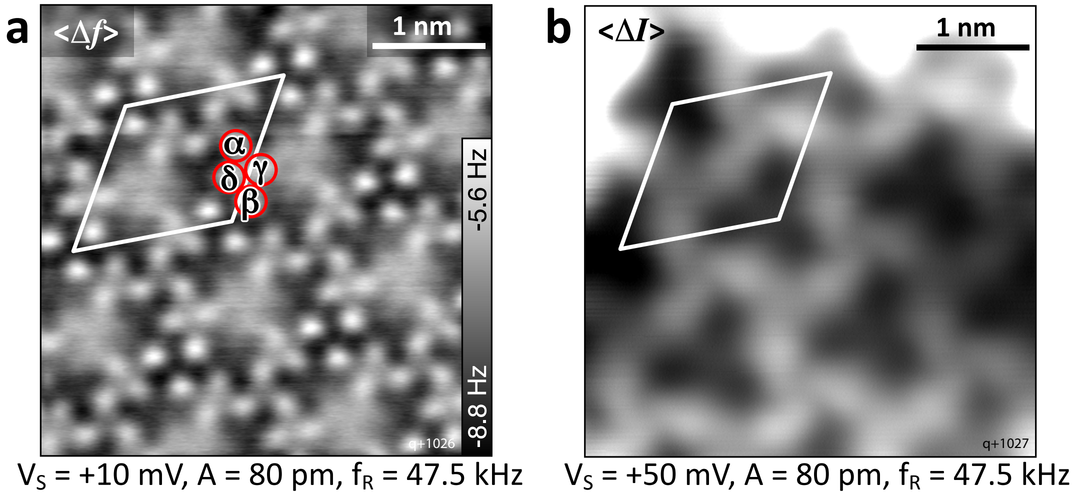

FIG. S 10: **O-terminated tip used for imaging the In_2O_3(111) surface** a) constant-height AFM image of the surface showing the surface O atoms. b) constant-height STM image of the same region showing contrast dominated by the In atoms.

In Fig. S10 we demonstrate the applicability of the oxygen-terminated TiO_2 tip in studying other oxide surfaces on the example of the In_2O_3(111) surface. The tip functionalization was performed on an O_2-covered TiO_2(110) surface in the same way it was functionalized for the AFM images of the main text. The sample was than switched to In_2O_3(111) and the resulting constant-height AFM image of the clean surface is seen in Fig. S10a. The bright features correspond to the terminating lattice oxygen atoms of the surface (four inequivalent sites, α–γ). The unit cell of the 3-fold symmetric surface containing 12 terminating O atoms is indicated on both panels. Fig. S10b displays the constant-height STM image of the same surface region as in Fig. S10a, where the appearance in empty states is typically without atomic resolution and determined by the differently coordinated In atoms – see the DOS in the Supplement of [2].

S 11. SI VIDEOS

Video S 1: **"TAU (peroxo) molecule tip approach"** Simulated AFM tip approach above the peroxo τ molecule. The left and middle panel display the animated tip approach from two different perspectives, while the right panel displays the measured force on the simulated tip at each point of the approach. The distance d is measured between the O atom at the simulated AFM tip apex and the adsorbate above which the force-curve is simulated, measured when both the tip and the sample are frozen.

Video S 2: **"PI (peroxo) molecule tip approach"** Simulated AFM tip approach above the peroxo π molecule. The left and middle panels display the animated tip approach from two different perspectives, while the right panel displays the measured force on the simulated tip at each point during the approach. The distance d is measured between the O atom at the simulated AFM tip apex and the adsorbate above which the force-curve is simulated, measured when both the tip and the sample are frozen.

Video S 3: **"OMEGA (peroxo) molecule tip approach"** Simulated AFM tip approach above the peroxo ω molecule. The left and middle panels display the animated tip approach from two different perspectives, while the right panel displays the measured force on the simulated tip at each point during the approach. The distance d is measured between the O atom at the simulated AFM tip apex and the adsorbate above which the force-curve is simulated, measured when both the tip and the sample are frozen.

Video S 4: **"ADATOM (doubly negative) tip approach"** Simulated AFM tip approach above the doubly negative oxygen adatom O_{ad}. The left and middle panels display the animated tip approach from two different perspectives, while the right panel displays the measured force on the simulated tip at each point during the approach. The distance d is measured between the O atom at the simulated AFM tip apex and the adsorbate above which the force-curve is simulated, measured when both the tip and the sample are frozen.

Video S 5: **"TAU (superoxo) molecule tip approach"** Simulated AFM tip approach above the superoxo τ molecule. The left and middle panels display the animated tip approach from two different perspectives, while the right panel displays the measured force on the simulated tip at each point during the approach. The distance d is measured between the O atom at the simulated AFM tip apex and the adsorbate above which the force-curve is simulated, measured when both the tip and the sample are frozen.

Video S 6: **"PI (superoxo) molecule tip approach"** Simulated AFM tip approach above the superoxo π molecule. The left and middle panels display the animated tip approach from two different perspectives, while the right panel displays the measured force on the simulated tip at each point during the approach. The distance d is measured between the O atom at the simulated AFM tip apex and the adsorbate above which the force-curve is simulated, measured when both the tip and the sample are frozen.

[1] P. Scheiber, A. Riss, M. Schmid, P. Varga, and U. Diebold, Physical Review Letters **105**, 216101 (2010).
[2] M. Wagner, S. Seiler, B. Meyer, L. A. Boatner, M. Schmid, and U. Diebold, Advanced Materials Interfaces **1**, 1400289 (2014).